Performance Limitations of Non-Laminated Magnetic Suspension Systems

Carl R. Knospe, *Senior Member, IEEE*, and Lei Zhu

***Abstract*—Limitations on the closed-loop performance of magnetic suspension systems employing electromagnetic actuators that are not constructed from laminations are examined. Eddy currents induced within the iron by time-varying magnetic fields are shown to have a strong effect on the system dynamics and hence the achievable performance. To obtain the needed relations, the theory of performance limitations, specifically the sensitivity integral constraint result, is extended to fractional order systems. The unstable pole of the plant and the achievable closed-loop bandwidth are then analytically determined as roots of a quintic polynomial. The results indicate that the required control effort increases as the square of flotor mass for actuators with significant eddy currents, while the relation is linear for laminated actuators.**

***Index Terms*—Active magnetic bearings, electromagnetic actuators, electromagnetic suspension, fractional order systems (FOSs), performance limits.**

I. Introduction

ELECTROMAGNETIC suspension systems are of interest for a variety of industrial and scientific applications that would benefit from their contact-free ability to manipulate objects. Among the applications studied are rotating machinery (i.e., active magnetic bearings) [1], metal conveyance [2], metal coating processes [3], photolithography [4], and tool servo systems [5].

In many applications, the electromagnet's stator and flotor (the manipulated part) are composed of laminations so as to reduce eddy currents within the ferromagnetic material. As Faraday's law dictates, eddy currents will be induced in any conductor in response to a changing magnetic field [6]. For electromagnetic suspension systems, the effect of eddy currents is a reduction in the time-varying component of the actuator force (an actuator gain reduction) as well as a phase lag between actuator coil current and the force produced. As both of these effects are detrimental to control system performance, laminated construction is typically used. In some applications, however, laminated construction is contradictory to the magnetic suspension's purpose (e.g., in sheet metal conveyance) or is precluded due to cost or strength concerns. An important example of the later is thrust magnetic bearings in rotating machinery, which rarely contain laminations. In such applications, eddy currents will have profound effects upon the behavior of the electromagnetic suspension system and must be considered in system modeling and controller design.

The goal of this paper is to examine the connection between non-laminated actuator design and the limits to achievable magnetic suspension performance. We will restrict our attention to the case of actuators with power amplifiers operated in current-mode. Modelling of non-laminated electromagnetic actuators has been previously examined in several studies [7]–[9]. Recently, the authors have developed accurate dynamic models for these actuators that link their transfer functions to geometric and material properties [10]–[12]. Herein, these transfer functions are examined via an extension of the *theory of performance limitations*.

Performance limitation theory establishes limits on what can and cannot be accomplished by a control system in terms of closed-loop performance, based on open loop plant characteristics. This theory began with the seminal work of Bode [13] in the 1940s, who used different contours of integration and integrands in Cauchy's theorem to derive a number of formulae that show the relationship between real and imaginary components of analytical functions. Horowitz gave interpretations of Bode's results in the context of control system design in the 1960s [14]. As an example, it has been shown that, if the open-loop system is a stable rational function with relative degree of at least two, then, provided the closed-loop system is stable, the sensitivity function must satisfy the following integral relation:

$$\int_0^\infty \log|S(j\omega)|\,d\omega = 0. \tag{1}$$

This integral dictates that the net area under the plot of $|S(j\omega)|$ on a logarithmic scale is zero. Therefore, the log area of those frequency ranges where $|S(j\omega)| > 1$ must equal that of those ranges where $|S(j\omega)| < 1$. This is a tradeoff between sensitivity amplification and attenuation. Due to the aforementioned balance of areas, the relation (1.15) is sometimes called the *area formula*.

Freudenberg and Looze extended Bode type integral constraints such as (1) to systems with open-loop unstable poles and time delays in the late 1980s [15], [16]. In 1991, Middleton developed Bode-type integrals for the complementary sensitivity function [17]. More recent investigations have focused on multivariable systems, sampled data systems, and nonlinear systems

Manuscript received January 02, 2009; revised April 15, 2009. Manuscript received in final form February 19, 2010. First published May 10, 2010; current version published February 23, 2011. Recommended by Associate Editor R. Moheimani. This work was supported by the National Science Foundation under Grant DMII-9988877.

C. R. Knospe is with the Department of Mechanical and Aerospace Engineering, University of Virginia, Charlottesville, VA 22904 USA (e-mail: knospe@virginia.edu).

L. Zhu is with the Calnetix, Cerritos, CA 90703 USA (e-mail: lzhu@ calnetix.com).

Color versions of one or more of the figures in this paper are available online at http://ieeexplore.ieee.org.

Digital Object Identifier 10.1109/TCST.2010.2044179

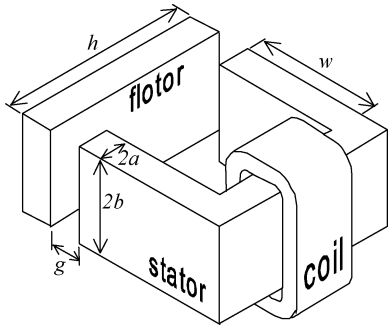

Fig. 1. Single C-core electromagnetic stator acting upon flotor, air gap g and geometrical parameters indicated.

[18]. For the analysis of non-laminated actuators we will provide a new extension of this theory for fractional order systems.

II. Preliminaries

A. Laminated Electromagnetic Suspensions

Our examination begins by reviewing electromagnetic suspension systems with laminated ferromagnetic components. Consider a single laminated electromagnetic stator acting upon a laminated flotor, as depicted in Fig. 1. The relationship between coil current i and force applied f is given by

$$f = \beta\left(\frac{N\,i}{g + g_{\text{eff}}}\right)^2 \tag{2}$$

where N is the number of coil turns; g is the gap between flotor and stator; g_{eff} is the effective air gap of the iron flux path (a parameter linearly dependent on the iron flux path length and inversely proportional to iron permeability); and β is a parameter dependent on actuator geometry and proportional to the actuator pole face area A. As the actuator can only pull upon the flotor, to achieve a stable suspension an opposing force must be provided by some other means, for example, by another actuator or by gravity acting upon the flotor. Thus, in equilibrium at a desired flotor position (gap length g_0), a bias force f_0 and current i_0 must be employed, where these quantities are related by

$$f_0 = \beta'\,\phi_0^2 \qquad \phi_0 = \frac{N\,i_0}{R^0} \tag{3}$$

where ϕ_0 is the bias flux; R^0 is the static reluctance of the flux path, which is an affine function of the nominal gap g_0; and parameter β' is dependent upon geometry. Both R^0 and β' are inversely dependent on pole face area.

Linearization of (3) about this equilibrium yields

$$f_p = K_i i_p + K_x x \tag{4}$$

where f_p, i_p, and x are variations in force, current, and gap from operating point values (f_0, i_0, g_0)

$$f_p = f - f_0 \qquad i_p = i - i_0 \qquad x = g_0 - g \tag{5}$$

and the coefficients are given by

$$K_i = \left.\frac{\partial f}{\partial i}\right|_{\substack{g=g_0\\ i=i_0}} > 0 \qquad K_x = \left.\frac{\partial f}{\partial x}\right|_{\substack{g=g_0\\ i=i_0}} > 0. \tag{6}$$

Variable i_p is commonly referred to as the perturbation current. We note that the actuator force f is directed opposite the positive direction for increasing gap. The positive direction for flotor displacement, x, is the same as the positive direction for actuator force f. (This choice of variables and axes is common in the literature.) The flotor displacement will be determined by the actuator force and the flotor compliance $H(s)$ via the relationship

$$X(s) = H(s)\ F_p(s) \tag{7}$$

where $F_p(s)$ and $X(s)$ are Laplace transforms of signals f_p and x. Equation (4) may be rewritten after Laplace transformation as

$$F_p(s) = K_i I_p(s) + K_x X(s) \tag{8}$$

where $I_p(s)$ is the Laplace transform of the perturbation current $I_p(s) = L\{i_p(t)\}$. Equations (7) and (8) form the conventionally-used model of a laminated electromagnetic suspension system (no eddy currents) operated in current mode.

B. Non-Laminated Electromagnetic Suspensions

For actuators composed partly or entirely of solid (i.e., *non-laminated*) ferromagnetic components, the model given in (8) is grossly inaccurate in practice due to the effect of eddy currents within the solid components [10]. As shown in [12], when eddy currents are significant, the model provided by (8) should be replaced with

$$F_p(s) = K_i \cdot \frac{R^0}{R^0 + c\sqrt{s}} I_p(s) + K_x \cdot \frac{R^0}{R^0 + c\sqrt{s}} X(s) \tag{9}$$

where c is an eddy current coefficient. In [10] and [11] the authors related parameters R^0 and c to actuator geometric and material properties. As coefficient c approaches zero (no eddy currents), the model of the laminated magnetic suspension system (8) is recovered. This model is appropriate when either the stator or flotor is not laminated, or in the case where both are not. The material and geometric properties of all components will affect R^0, however c will be dependent only on those of the non-laminated components [24]. Experimental results have shown that the model (9) is highly accurate [12], [24]. Both models (8) and (9) were obtained via linearization about the equilibrium. The range of gap variation over which these models are valid representations is dependent on the actuator employed, in particular on the reluctance of the iron path. In the authors' experience, linearization is typically valid over 25% of the nominal gap.

We note that the parameters K_i and K_x in (9) are the same as those found for the case of a laminated actuator and are given by

$$K_i = \frac{K_\phi N}{R^0} \qquad K_x = \frac{K_\phi^2}{R^0}. \tag{10}$$

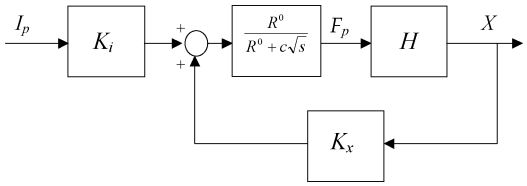

Fig. 2. Block diagram of a non-laminated electromagnetic suspension system operated in current mode.

In this result, $K_\phi = F_p(s)/\phi_p(s)$, where $\phi_p(s)$ is the Laplace transform of the perturbation flux signal. We note that $K_\phi \propto \phi_0/A$, where A is the pole face area.

A block diagram model of a non-laminated actuator operated in current mode is illustrated in Fig. 2. The transfer function from perturbation current to flotor displacement is

$$\frac{X(s)}{I_p(s)} = \frac{K_i R^0 H(s)}{c\sqrt{s} + R^0 - K_x R^0 H(s)}. \tag{11}$$

Throughout the remainder of this paper we will treat the case of a rigid flotor with no mechanical contact, hence the flotor compliance is given by the transfer function

$$H(s) = \frac{1}{ms^2}$$

where m is the flotor mass. This is a typical model for many applications, including metal conveyance and the thrust bearing axis of levitated rotors.

With the introduction of the electromagnetic and flotor time constants (T_{em} and T_f, respectively)

$$T_{em} = \left(\frac{c}{R^0}\right)^2 \qquad T_f = \sqrt{\frac{m}{K_x}} \tag{12}$$

the plant transfer function may be written as

$$P(s) = \frac{X(s)}{I_p(s)} = \frac{\frac{K_i}{m}}{\sqrt{T_{em}}s^{5/2} + s^2 - \frac{1}{T_f^2}}. \tag{13}$$

For example, consider the C-core electromagnetic actuator with geometry shown in Fig. 1. Denote pole face area as A and iron path length as l ($l = 2w+2h$). From [11], the coefficients of the transfer function model are given by the analytic expressions

$$K_\phi = \frac{1}{\mu_0}\left(\frac{2}{A}\right)\cdot\frac{N\,i_0}{R^0} \tag{14a}$$

$$R^0 = \frac{1}{\mu_0 A}\left(2g_0 + \frac{l}{\mu_r}\right) \tag{14b}$$

$$c = \psi(\varepsilon_a, \varepsilon_b)\cdot\sqrt{\frac{\sigma}{\mu_r\mu_0}}$$

$$\psi(\varepsilon_a, \varepsilon_b) = \left[\frac{1}{4(\varepsilon_a+\varepsilon_b)} + \frac{1}{3}\frac{\varepsilon_b}{\varepsilon_a} - \frac{64}{\pi^5}\frac{\varepsilon_b^2}{\varepsilon_a^2}\tanh\left(\frac{\pi}{2}\frac{\varepsilon_a}{\varepsilon_b}\right)\right] \tag{14c}$$

with nondimensional parameters ε_a and ε_b dependent on actuator geometry

$$\varepsilon_a = \frac{a}{l} \qquad \varepsilon_b = \frac{b}{l}.$$

It is straightforward to show that

$$K_\phi^2 = \frac{2f_0}{\mu_0 A} \qquad K_x = \frac{4f_0}{2g_0 + \frac{l}{\mu_r}}. \tag{15}$$

Similar relationships are available for other geometries (e.g., E-core, cylindrical).

III. Fractional Order Systems

A. Introduction

The analytic model (13) presents an unusual type of transfer function as the powers of the complex frequency variable s in the denominator are not all integers. This system belongs to a class of transfer functions in form of

$$F(\sqrt[n]{s}) = \frac{b_m s^{m/n} + b_{m-1}s^{(m-1)/n} + \cdots + b_1 s^{1/n} + b_0}{s^{l/n} + a_{l-1}s^{(l-1)/n} + \cdots + a_1 s^{1/n} + a_0} \tag{16}$$

with n, l, and m being positive integers with $l \geq m$. A system in the form of (16) is known as a *fractional order system* (FOS) [19], [20]. Function s^α is the frequency domain analog to a time domain operator d^α/dt^α. For $\alpha < 0$, the operator is a *fractional integral* of order α, while for $\alpha > 0$, it is a *fractional derivative* of order α [19]–[21]. Here, we specify that the argument of complex frequency satisfy $\arg(s) \in (-\pi, \pi)$ so as to be consistent with physical meaning and guarantee a unique value of $F(\sqrt[n]{s})$.

B. Stability Criteria for Fractional Order Systems

In 1996, Matignon presented a conjecture regarding the bounded-input-bounded-output (BIBO) stability of FOS [22]. This conjecture was proven by Bonnet and Partington in 2000 [23]. A useful restatement of this result was provided by Zhu [24].

Theorem 1: Consider a fractional order system $F(\sqrt[n]{s})$ in the form (16), in which no cancellation occurs between D_F and N_F in the closed right half plane. Suppose the denominator can be written as

$$D_F\left(\sqrt[n]{s}\right) = \prod_{i=1}^{h}\left(\sqrt[n]{s} - \lambda_i\right)^{k_i} \tag{17}$$

where $k_i > 0$, $l > 0$, and $\sum_{i=1}^{h} k_i = l$. Then F is *BIBO* stable if and only if for every λ_i

$$|\arg(\lambda_i)| > \frac{\pi}{2n}. \tag{18}$$

Note that the λ_i are roots of the polynomial

$$z^l + a_{l-1}z^{(l-1)} + \cdots + a_1 z^1 + a_0 = 0$$

which is achieved from (17) via $z = \sqrt[n]{s}$.

C. Bode Sensitivity Integral Constraint

The following results for FOSs are natural extensions of Freudenberg and Looze's work in [16]. These results indicate the performance limitations caused by the unstable poles of an open-loop fractional order system.

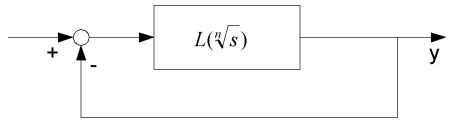

Fig. 3. Closed-loop FOS.

Theorem 3: Consider a stable closed-loop FOS shown in Fig. 3. Suppose that the loop gain $L(\sqrt[n]{s})$ has a relative degree greater than 1 and has k unstable poles, where repeated unstable poles are counted according to their multiplicity. Then, the integral of the system's sensitivity function along the frequency axis is

$$\int_0^{+\infty} \log\left|S\left(\sqrt[n]{i\omega}\right)\right| d\omega = \pi \sum_{j=1}^{k} \lambda_j^n \tag{19}$$

where $\lambda_1^n, \ldots, \lambda_k^n$ are the unstable poles of the loop gain.

Proof: The proof of this result is provided in [24]. □

Since the summation term on the right side of (19) is positive, Theorem 3 shows that unstable open-loop poles of a fractional order system break the otherwise balance between the areas of sensitivity reduction and amplification, and increase the contribution of the frequency range of amplification to the integral in (19). Moreover, the farther from the imaginary axis the unstable poles are, the more pronounced this increase.

Theorem 3 presents a fundamental limitation on performance of the closed-loop fractional order control system since it has only been assumed that the closed-loop system is stable, and that the relative degree of the loop gain is greater than 1. The stability assumption is natural consequence of our interest in an operable closed loop system. The relative degree assumption is always true in any practical application where sensors and amplifiers always have limited bandwidth. No assumption is made on the form of the controller used beyond that it is a linear FOS.

One cannot conclude any meaningful design limitation from Theorem 3 itself, since distributing a sensitivity amplification of slightly greater than one over an arbitrarily large frequency range can provide the area necessary for the positive contribution to the integral in (19). However, practical issues such as unmodeled dynamics at higher frequencies, sensor noise, and realizable control bandwidth prevent such a distribution in practice. The loop gain of a FOS must decrease with increasing frequency. It is reasonable to assume, as Freudenberg and Looze have done for integer order systems, that the loop gain of a FOS satisfies a design specification of the type

$$\left|L(\sqrt[n]{j\omega})\right| \leq \varepsilon\left(\frac{\omega_c}{\omega}\right)^{1+k} \qquad \forall \omega \geq \omega_c \tag{20}$$

where $\varepsilon < 1/2$, and k is a positive fraction. This assumption characterizes the bandwidth and roll-off rate of the loop gain. As pointed out in [18], the value of ω_c will be quite close to that of the closed loop bandwidth ω_{bw}, which is defined as the highest frequency where

$$\left|\frac{L\left(\sqrt[n]{j\omega_{bw}}\right)}{1+L\left(\sqrt[n]{j\omega_{bw}}\right)}\right| = \frac{\sqrt{2}}{2}.$$

As a result, ω_c will be referred to in this paper as the *closed-loop bandwidth*.

Corollary 1: Suppose that the loop gain $L(\sqrt[n]{s})$ satisfies the bandwidth restriction (20). Then

$$\left|\int_{\omega_c}^{+\infty} \log\left|S(\sqrt[n]{j\omega})\right| d\omega\right| \leq \frac{3\varepsilon\omega_c}{2k}. \tag{21}$$

Proof: The result can be achieved in the same manner as that of Corollary 3 in [16]. However, note that in [16], k is a positive integer while in (21) it may be specified as any positive fraction. See [24] for details. □

The corollary indicates that a reduction in sensitivity at low frequency will necessitate a peak in sensitivity at higher frequency.

Let us now consider the tracking a reference signal. This may be considered in the frequency domain as requiring the sensitivity function of the FOS to be small over a low frequency band

$$\left|S\left(\sqrt[n]{j\omega}\right)\right| \leq \underline{S} < 1, \quad \forall \omega \leq \omega_a < \omega_c \tag{22}$$

where frequency ω_a will be referred to as the *attenuation bandwidth* and $\underline{S}$ is the specified sensitivity bound.

Suppose from a design standpoint that a target value of peak sensitivity is prescribed, which we will denote by

$$\overline{S} = \sup_{\omega\in[\omega_a,\omega_c]} \left|S\left(\sqrt[n]{j\omega}\right)\right|. \tag{23}$$

Combining (19), (21) and (22), it is straightforward to demonstrate that

$$\omega_c\left(\log\left(\overline{S}\right) + \frac{3\varepsilon}{2k}\right) - \pi\sum_{j=1}^{k}\lambda_j^n \geq \omega_a\,\Delta\log\left(S\right) \tag{24}$$

where $\Delta\log(S)$ is the change in the log sensitivity desired from the attenuation band to the peak, i.e.,

$$\Delta\log\left(S\right) = \log\left(\overline{S}\right) - \log\left(\underline{S}\right) = \log\left(\frac{\overline{S}}{\underline{S}}\right).$$

The right-hand side of Inequality (24) is the shaded area depicted in Fig. 4. The result (23) shows that as the sensitivity over the frequency band $[0, \omega_a]$ is reduced (i.e., smaller $\underline{S}$), the peak in sensitivity over the frequency range $[\omega_a, \omega_c]$ must increase no matter what stabilizing controller is employed. Furthermore, the sensitivity peak must also be amplified if the frequency range of sensitivity reduction $[0, \omega_a]$ is enlarged. Thus, the design constraint imposed by the sensitivity integral (19) is evident. Note that increasing the closed-loop bandwidth (ω_c) will lower the cost of low frequency sensitivity reduction.

Equation (24) may be alternately expressed as

$$\omega_c > \kappa\,\omega_a + \beta\sum_{j=1}^{K}\lambda_j^n$$

where

$$\kappa = \frac{\Delta\log\left(S\right)}{\log\left(\overline{S}\right) + \frac{3\varepsilon}{2k}} \qquad \beta = \frac{\pi}{\log\left(\overline{S}\right) + \frac{3\varepsilon}{2k}}.$$

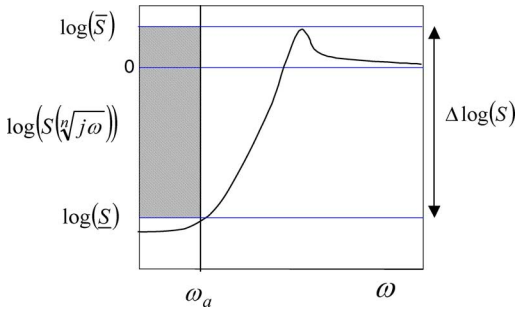

Fig. 4. Area related to control system performance.

This specifies the needed closed-loop bandwidth as a linear combination of the desired attenuation bandwidth and sum of the plant's unstable poles, the coefficients of the relation (κ, β) dependent on the sensitivities specified. A necessary condition for the closed-loop bandwidth is

$$\omega_c > \kappa \omega_a. \tag{25}$$

We now turn our attention to relating closed-loop bandwidth ω_c and unstable poles λ_j^n to the parameters in the non-laminated system model (13).

IV. Unstable Poles of the Plant

A. Single Unstable Pole

The characteristic polynomial derived from the denominator of the plant's transfer function (13) is given by

$$\sqrt{T_{em}} z^5 + z^4 - \frac{1}{T_f^2} = 0 \tag{26}$$

where $z = \sqrt{s}$. The roots of this polynomial, denoted λ_i, determine stability according to Theorem 1, the stability condition being

$$|\arg(\lambda_i)| > \frac{\pi}{4} \qquad \forall i. \tag{27}$$

The unstable roots also play an important role in the performance limitation specified in (24). Here, we will prove that (26) has precisely one root violating (27) and develop an analytic solution for this root. Clearly, $\lambda_i = 0$ is not a root of (26). Therefore, we let $\chi = z^{-1}$ and multiply (26) by χ^5 to obtain

$$\chi^5 - T_f^2 \chi - T_f^2 \sqrt{T_{em}} = 0.$$

Using the transformation $\chi = \sqrt{T_f}\nu$ results in an equation in Bring-Jerrard Quintic Form [25], [26]

$$\nu^5 - v - \rho = 0 \tag{28}$$

with

$$\rho = \sqrt{\frac{T_{em}}{T_f}}. \tag{29}$$

Note that $\rho = 0$ corresponds to the case of no eddy currents.

Since the conversion from z to ν involves only inversion and scaling, roots of (26) which satisfy condition (27) will correspond to roots of (28) that also satisfy (27). Furthermore, roots of (26) that violate condition (27) will correspond to roots of (28) that violate condition (27). Finally, note that zero is not a root of (28) for $\rho > 0$.

Lemma 1: For $\rho > 0$, (28) has a single root denoted ν_+ satisfying $|\arg(\nu_+)| \leq \pi/4$ and this root is a positive real number greater than one.

Proof: Equation (28) may be rewritten as

$$\nu^4 (v - 1) = \rho. \tag{30}$$

Taking the argument of this equation yields

$$4 \arg(\nu) + \arg(v - 1) = 2\pi k, \quad k = \cdots -2, -1, 0, 1, 2 \ldots \tag{31}$$

where $\arg(\rho) = 2\pi k$ since $\rho > 0$. Since the coefficients of (28) are real, all complex roots will appear as complex conjugate pairs. Therefore, to analyze stability we need to only consider roots in the octant $0 \leq \arg(\nu) \leq \pi/4$. Consider first the case $0 < \arg(\nu) \leq \pi/4$. Then

$$0 < \arg(v) < \arg(v - 1) < \pi$$
$$0 < 4 \arg(v) \leq \pi.$$

Thus, (31) has no solution within $0 < \arg(\nu) \leq \pi/4$ and so (28) does not either. Now consider the case where $\arg(\nu) = 0$, that is, where ν is a positive real number. If $0 < \nu < 1$ then $\arg(\nu - 1) = \pi$ and (31) will have no solution. For any $\nu > 1$, $\arg(\nu - 1) = 0$ and (31) will be satisfied. Therefore, if a root ν_i of (28) has $|\arg(\nu_i)| \leq \pi/4$, it must be a real number larger than one. Equation (30) may be alternatively expressed as

$$\nu^4 = \frac{\rho}{\nu - 1}.$$

Since the left-hand side of this equation is monotonically increasing from one to infinity on $1 < \nu < \infty$ while the right-hand side is monotonically decreasing from infinity to zero over the same domain, the equation has one and only one root on $1 < \nu < \infty$. □

The single positive real root ν_+ of (28) corresponds to a positive real root of (26), denoted λ_+.

B. Analytic Solution

The general quintic equation is not solvable algebraically in terms of a finite number of additions, multiplications, and root extractions. Nevertheless, an analytic solution is available for Bring-Jerrard Quintic Form [26] in terms of the generalized hypergeometric function

$${}_4F_3 \left[\begin{matrix} a_1, a_2, a_3, a_4 \\ b_1, b_2, b_3 \end{matrix} \; ; \; y \right] = \sum_{k=0}^{\infty} \frac{(a_1)_k (a_2)_k (a_3)_k (a_4)_k \, y^k}{(b_1)_k (b_2)_k (b_3)_k \, k!}$$

where $(a)_k$ are Pochhammer symbols

$$(a)_k \equiv a(a+1)\cdots(a+k-1).$$

The positive real root of (28) is given by

$$\nu_+ = J_+(\rho)$$

where

$$\begin{aligned} J_+(\rho) = {}& {}_4F_3\left[\begin{matrix}\frac{-1}{20},\frac{3}{20},\frac{7}{20},\frac{11}{20}\\ \frac{1}{4},\frac{1}{2},\frac{3}{4}\end{matrix}\ ;\ \tfrac{3125}{256}\rho^4\right] \\ & + \frac{\rho}{4}{}_4F_3\left[\begin{matrix}\frac{1}{5},\frac{2}{5},\frac{3}{5},\frac{4}{5}\\ \frac{1}{2},\frac{3}{4},\frac{5}{4}\end{matrix}\ ;\ \tfrac{3125}{256}\rho^4\right] \\ & - \frac{5}{32}\rho^2{}_4F_3\left[\begin{matrix}\frac{9}{20},\frac{13}{20},\frac{17}{20},\frac{21}{20}\\ \frac{3}{4},\frac{5}{4},\frac{3}{2}\end{matrix}\ ;\ \tfrac{3125}{256}\rho^4\right] \\ & + \frac{5}{32}\rho^3{}_4F_3\left[\begin{matrix}\frac{7}{10},\frac{9}{10},\frac{11}{10},\frac{13}{10}\\ \frac{5}{4},\frac{3}{2},\frac{7}{4}\end{matrix}\ ;\ \tfrac{3125}{256}\rho^4\right]. \end{aligned} \quad (32)$$

Transformation back to the z-domain yields the positive real root of (26)

$$\lambda_+ = \frac{1}{\sqrt{T_f}\, J_+(\rho)}.$$

In terms of the s-plane, the pole is represented by

$$\lambda_+^2 = \frac{1}{T_f\{J_+(\rho)\}^2} = \frac{1}{\left\{J_+\left(\sqrt{\frac{T_{em}}{T_f}}\right)\right\}^2}\sqrt{\frac{K_x}{m}}. \quad (33)$$

In the case of no eddy currents ($T_{em} = 0$), this result reduces to the correct value for a laminated magnetic suspension, $\sqrt{K_x/m}$, as $J_+(0) = 1$.

Lemma 2: $J_+(\rho)$ is an increasing function for $\rho > 0$.

Proof: $\nu_+ = J_+(\rho)$ satisfies $\nu_+^5 - \nu_+ = \rho$. Hence, $d\nu_+/d\rho = 1/(5\nu_+^4 - 1)$. Since $\nu_+ > 1$ for $\rho > 0$, we have $d\nu_+/d\rho > 0$. □

Lemma 2 has the following consequence. Since $J^+(\rho)$ is an increasing function of ρ, as the eddy current parameter c is increased the unstable pole moves continuously closer to the origin (i.e., decreasing $(\lambda^+)^2$). This pole motion results in the relaxation of the constraint on $\omega_a\ \Delta\log(S)$ provided by Inequality (24). Thus, in terms of pole location alone, eddy currents act to allow *higher performance* for the closed-loop system. As we will see, this advantage is offset by the penalty incurred from lowered achievable closed-loop bandwidth.

Note that the inverse function of J_+ exists for real $\nu_+ > 1$ and is trivially defined

$$\rho = J_+^{-1}(\nu) \qquad J_+^{-1}(\nu) = \nu^5 - \nu.$$

V. Achievable Bandwidth

A. Controller Gain Constraint

We now will investigate the link between achievable closed-loop bandwidth, ω_c, and the parameters in non-laminated system model (13). Such a link arises from the impossibility in practice of the controller achieving loop gain crossover at an arbitrarily high frequency in spite of the roll-off in the actuator's gain resulting from eddy currents. To capture this reality, we introduce a constraint on the allowable controller's gain

$$|K_i C(j\omega)| \le \gamma \qquad \forall\omega > \omega_a. \quad (34)$$

The constraint is not imposed at lower frequencies since the controller may contain an integrator. Since $|K_i C(j\omega)|$ has units of force/displacement, γ may be considered a bound on the maximum dynamic stiffness for higher frequencies. We will refer to it herein as the *control effort*. Such bounds are often employed in controller synthesis for magnetic suspension systems [1]. The allowable value for γ is dependent on many factors including sensor noise, amplifier hardware, and the accuracy of the model to be employed in design.

B. Closed-Loop Bandwidth

Consider the gain plot depicted in Fig. 5. Schematically shown as a function of frequency are the plant's gain, a desirable loop gain for compensation, and the loop gain constraint (20). On the log scale used, the gain of the controller is the difference between that of the loop gain and that of the plant. Note that the plant's gain curve has a high frequency slope of $-2(1/2)$ decade/decade, as dictated by (13). In contrast, the loop gain has a high frequency slope more negative than this as the controller must roll-off at high frequency. In the immediate vicinity of ω_c the loop gain slope matches that of constraint (20), hence it is $-(1+k)$ decade/decade here. Clearly, $k \ge 3/2$ to limit controller gain in this frequency range. Below this frequency range, the loop gain slope will be between -1 and $-1(1/2)$; decade/decade to ensure good phase margin at the loop crossover frequency ω_{lc}. To ensure adequate phase margin, the loop crossover frequency ω_{lc} should not be too close to the closed-loop bandwidth frequency ω_c. To this end, parameter ε in constraint (20) should be assumed to be in the range 0.1 to 0.2. Since the plant's gain rolls off with a slope less than -2 decade/decade in the frequency range $[\omega_{lc}, \omega_c]$ while the loop gain's slope is greater than $-1(1/2)$; decade/decade in this same band, we may conclude that, as a general rule, the controller gain will increase up to frequency ω_c. Therefore, for performance analysis we may replace Constraint (34) by the inequality

$$|K_i C(j\omega_c)| \le \gamma. \quad (35)$$

Note that $C(s) = L(s)/P(s)$ and therefore

$$K_i C(s) = L(s)\left\{\sqrt{T_{em}}s^{5/2} + s^2 - \frac{1}{T_f^2}\right\}m.$$

For the performance limitation analysis we have $|L(j\omega_c)| \le \varepsilon$. We will treat this relation as an equality since we seek to maximize ω_c. Hence (35) is equivalent to (after some algebra)

$$\left\{\frac{\sqrt{2}}{2}\sqrt{T_{em}}{\omega_c}^{5/2} + {\omega_c}^2 + \frac{1}{T_f^2}\right\}^2 + \left\{\frac{\sqrt{2}}{2}\sqrt{T_{em}}{\omega_c}^{5/2}\right\}^2 \le \left\{\frac{\gamma}{\varepsilon m}\right\}^2. \quad (36)$$

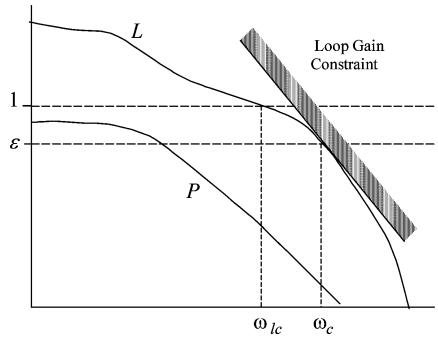

Fig. 5. Illustrative frequency response diagram of loop gain (L), plant gain (P), and constraint (20) on log-log scale. The logarithm of controller gain is the difference between the L and P curves.

C. Upper Bound

As (36) is a tenth order inequality in $\omega_c^{1/2}$, some approximation will be necessary if an analytic result is to be obtained which ties achievable closed-loop bandwidth to the electromagnetic time constant of the non-laminated actuator. Unfortunately, with typical values of the variables, all terms in this expression are more or less of the same magnitude and simplification cannot be realized by simply dropping small terms.

We note that (36) is of the form

$$M^2 + N^2 \leq \Gamma^2 \qquad 0 \leq M < N \tag{37}$$

with

$$M = \left\{ \frac{\sqrt{2}}{2} \sqrt{T_{em}} {\omega_c}^{5/2} \right\}$$
$$N = \left\{ \frac{\sqrt{2}}{2} \sqrt{T_{em}} {\omega_c}^{5/2} + {\omega_c}^2 + \frac{1}{T_f^2} \right\}$$
$$\Gamma = \frac{\gamma}{\varepsilon m}.$$

We will strengthen the condition (37) slightly to the linear constraints

$$N + M \leq \sqrt{2}\Gamma \qquad 0 \leq M < N. \tag{38}$$

This will result in an estimate of ω_c that is larger than the actual value. This upper bound on ω_c will be denoted $\overline{\omega}_c$. In Appendix I we show that this upper bound is sufficiently tight that it may be employed in performance analysis.

Since the second condition of (38) is automatically satisfied for any $\omega_c > 0$, only the first constraint is necessary. This translates to

$$\sqrt{2T_{em}} {\omega_c}^{5/2} + {\omega_c}^2 + \frac{1}{T_f^2} \leq \sqrt{2} \frac{\gamma}{\varepsilon m}. \tag{39}$$

To find the maximum $\overline{\omega}_c$ achievable, we solve the equality

$$\sqrt{2T_{em}} {\overline{\omega}_c}^{5/2} + {\overline{\omega}_c}^2 + \frac{1}{T_f^2} = \sqrt{2} \frac{\gamma}{\varepsilon m}. \tag{40}$$

Noting that $\overline{\omega}_c > \omega_c$ and combining (25) and (40) yields an inequality on control effort

$$\gamma > \gamma_{\min}$$

where the minimum control effort required to achieve the specified sensitivities and attenuation band is

$$\gamma_{\min} = \left[\varepsilon \, \kappa^{5/2} \, \omega_a^{5/2} \right] \, m \sqrt{T_{em}} + \{\gamma_{\min}\}_{lam} \tag{41}$$

and $\{\gamma_{\min}\}_{lam}$ is the minimum control effort required with a laminated actuator (i.e., no eddy currents)

$$\{\gamma_{\min}\}_{lam} = \left[\varepsilon \frac{\sqrt{2}}{2} \left(\kappa^2 \omega_a^2 + \frac{1}{T_f^2} \right) \right] \, m. \tag{42}$$

Note from (41) that the minimum control effort required with eddy currents is greater than that without, all other variables held equal.

Returning now to determining bandwidth as a function of actuator parameters, we denote a time constant associated with the control effort as

$$T_\gamma = \sqrt{\frac{\varepsilon m}{\gamma}}. \tag{43}$$

Employing the changes of variables $\chi_c = 1/\sqrt{\overline{\omega}_c}$, (40) yields

$$\left(\sqrt{2} \frac{1}{T_\gamma^2} - \frac{1}{T_f^2} \right) \chi_c^5 - \chi_c - \sqrt{2T_{em}} = 0.$$

We note that for any realistic suspension system $T_f \gg T_\gamma$ and therefore we may examine the simplified equation

$$\chi_c^5 - \sqrt{\frac{1}{2}} T_\gamma^2 \chi_c - T_\gamma^2 \sqrt{T_{em}} = 0. \tag{44}$$

The transformation $\chi_c = (1/2)^{1/8} {T_\gamma}^{1/2} \nu_c$ applied to (44) results in an equation in Bring-Jerrard Quintic Form

$$\nu_c^5 - \nu_c - \rho_c = 0 \tag{45}$$

where

$$\rho_c = 2^{5/8} \sqrt{\frac{T_{em}}{T_\gamma}}. \tag{46}$$

Since we seek the positive real root of (40) and the transformation from $\overline{\omega}_c$ to ν_c involves only inversion and scaling, the positive real solution of (45) is of interest; this is given by

$$\nu_c = J_+ (\rho_c).$$

Transformation of this result back to $\overline{\omega}_c$ yields

$$\overline{\omega}_c = \frac{2^{1/4}}{T_\gamma \{J_+ (\rho_c)\}^2}. \tag{47}$$

The necessary condition on attenuation bandwidth is

$$\omega_a < \frac{1}{\kappa}\,\frac{2^{1/4}}{T_\gamma\{J_+(\rho_c)\}^2}. \tag{48}$$

D. Discussion

Determining achievable closed-loop bandwidth given system parameters c, R^0, m, and control effort γ requires finding the positive root of a fifth-order polynomial. The problem of analytically connecting system data to closed loop bandwidth is fundamentally difficult in this sense. This is also true for the attenuation bandwidth ω_a. On the other hand, the problem of characterizing actuators (i.e., c and R^0) for which a given bandwidth $\overline{\omega}_c$ and control effort γ are feasible is more straightforward. From (39) we have

$$\frac{c}{R^0} = \sqrt{T_{em}} \le \frac{1}{\sqrt{2}\,\overline{\omega}_c{}^{5/2}}\left(\sqrt{2}\frac{\gamma}{\varepsilon\, m} - \frac{1}{T_f^2} - \overline{\omega}_c{}^2\right). \tag{49}$$

If the control effort is held constant, (49) indicates that as the effect of eddy currents increases (i.e., c) the closed-loop bandwidth $\overline{\omega}_c$ must decrease.

VI. Performance Limitations

A. Actuator Area and Gap

Employing (25), relationship (49) provides a necessary condition for the actuator to be capable of achieving the specified attenuation bandwidth, control effort, and sensitivities

$$\frac{c}{R^0} < \frac{1}{\sqrt{2}\,\kappa^{5/2}\omega_a{}^{5/2}}\left(\sqrt{2}\frac{\gamma}{\varepsilon\, m} - \frac{1}{T_f^2} - \kappa^2\omega_a{}^2\right). \tag{50}$$

Since $T_f \gg T_\gamma$, the inequality can be simplified to

$$\frac{c}{R^0} < \frac{1}{\sqrt{2}\,\kappa^{5/2}\omega_a{}^{5/2}}\left(\sqrt{2}\frac{\gamma}{\varepsilon\, m} - \kappa^2\omega_a{}^2\right) \tag{51}$$

allowing the right-hand side to depend on only performance specifications (i.e., independent of actuator geometry and materials), and the left hand side to depend on only actuator geometry and materials (i.e., independent of performance specifications). Consider the C-core actuator depicted in Fig. 1. The left-hand side of (51) can be expressed as

$$\frac{c}{R^0} = A\frac{\psi(\varepsilon_a,\varepsilon_b)}{2\mu_r g_0 + l}\sqrt{\sigma\mu_0\mu_r}. \tag{52}$$

To maximize achievable attenuation bandwidth, the actuator should be designed so as to minimize pole face area. Of course, the area must be sufficient to supply the peak force required for the application, denoted f_{peak}. The pole face area must satisfy

$$A > \frac{\mu_0 f_{\rm peak}}{B_{\rm sat}^2}$$

where $B_{\rm sat}$ is the saturation flux density of the iron (1.6 T for silicon iron, 2.0 T for cobalt iron). Another approach to improving attenuation bandwidth in design according to (51) and (52) is to increase the air gap g_0. However, this would require a larger actuator with more ampere-turns, which may be impractical. It should be noted that we have assumed an ideal transconductance amplifier model in this study and that any hardware-specific dependence of amplifier bandwidth upon actuator design is not captured in the model employed in this paper.

B. Scaling With Flotor Mass

We now examine the question of how the necessary control effort γ scales with the mass of the flotor m. For this analysis, we will make three assumptions.

1) The flotor is levitated by a magnetic actuator positioned above it (single-sided suspension) with the opposing force supplied by gravity. In this case, the bias force f_0 and flux ϕ_0 are dictated by the flotor mass.
2) The actuator is sized such that the bias flux density B_0 is held constant between designs. This is a natural assumption if one is considering varying flotor mass by orders of magnitude as the maximum value of flux density is limited by magnetic saturation in the iron.
3) The nominal gap g_0 between the actuator and the flotor is held fixed among designs.

Assumption 1 implies that $f_0 \propto m$ while Assumption 2 provides $\phi_0 \propto A$. From (3) we have $\phi_0 \propto m$ and therefore $A \propto m$. Noting that $R_0 \propto A^{-1}$ and $c \propto A^0$ (i.e., independent of A), we find

$$R^0 \propto m^{-1}c \propto m^0\sqrt{T_{em}} = \frac{c}{R^0} \propto m.$$

Since $K_\phi \propto \phi_0/A$, it is independent of m. Therefore, from (10) we have

$$K_x \propto \frac{1}{R^0} \propto m$$

and we find $T_f = \sqrt{m/K_x}$ is independent of mass. Hence, $\rho = \sqrt{T_{em}/T_f} \propto m$. Since $J_+(\rho)$ has a weak dependence on ρ (note that $J_+(\rho)$ scales as $\rho^{1/5}$ for $\rho > 1$), (33) shows that λ_+^2 is weakly dependent on m.

The terms in the square brackets in (41) and (42) are independent of flotor mass. As a result, (42) indicates that the minimum control effort for a laminated actuator scales linearly with flotor mass when the attenuation band ω_a and sensitivity specifications are held fixed. In the case of a non-laminated actuator, however, the minimum control effort scales as m^2, as indicated by (41), noting that $\sqrt{T_{em}} \propto m$.

VII. Conclusion

The closed-loop performance of magnetic suspension systems with non-laminated actuators are strongly affected by the presence of eddy currents in the iron components. In this paper, the connection between the coefficients of a fractional order transfer function model of these actuators and the achievable closed-loop performance is studied. First, an extension of sensitivity integral performance limitations to the case of fractional order systems is provided. The unstable open-loop pole of the plant is then expressed as an analytic function of the problem data. An upper bound on the achievable closed-loop bandwidth

is also expressed analytically in terms of this data. The gap between this upper bound and the achievable bandwidth is analyzed and the upper bound is found to be of acceptable accuracy. The family of actuators for which there exists a controller satisfying the design specifications (i.e., attenuation band, minimum and maximum sensitivity, control effort) was determined. Finally, the scaling of the control effort required with the flotor mass was examined. It was found that control effort must increase with increased flotor mass at a rate more rapid than linear for non-laminated systems.

APPENDIX

In examining the quality of the upper bound (47), let us first consider the case of a laminated actuator (i.e., no eddy currents, $T_{em} = 0,\ \rho_c = 0$). The closed-loop bandwidth provided by (47) in this case is given by

$$\{\overline{\omega}_c\}_{lam} = 2^{1/4}\sqrt{\frac{\gamma}{m\,\varepsilon}}.$$

This value is slightly higher (19%) than the actual closed-loop bandwidth achievable, $\{\omega_c\}_{lam} = \sqrt{\gamma/m\,\varepsilon}$. For the general case ($T_{em} \neq 0$), we will develop two lower bounds on ω_c so as to assess the tightness of the upper bound. Using (40), letting $\overline{z} = \overline{\omega}_c^{1/2}$, and dropping the small T_f^{-2} term (as previously), yields

$$\sqrt{T_{em}}\overline{z}^5 + \frac{\sqrt{2}}{2}\overline{z}^4 - \Gamma = 0 \tag{A1}$$

which has the positive real solution $\lambda_c = \sqrt{\overline{\omega}_c}$ and therefore

$$\sqrt{T_{em}}\lambda_c^5 + \frac{\sqrt{2}}{2}\lambda_c^4 - \Gamma = 0. \tag{A2}$$

A lower bound $\underline{\omega}_c$ may be developed by solving $N+M=\Gamma$ as this curve lies within $N^2 + M^2 \leq \Gamma^2$. Let $\underline{z} = \underline{\omega}_c^{1/2}$. Then, $N + M = \Gamma$ may be written as

$$\sqrt{T_{em}}\underline{z}^5 + \underline{z}^4 - \Gamma = 0. \tag{A3}$$

Employing the change of variables $\delta = \underline{z} - \lambda_c$, (A3) becomes

$$\begin{aligned} b_5\delta^5+b_4\delta^4+b_3\delta^3+b_2\delta^2+b_1\delta+b_0=0 \\ b_5 &= \sqrt{T_{em}} \\ b_4 &= \left(5\sqrt{T_{em}}\lambda_c + 1\right) \\ b_3 &= \left(10\sqrt{T_{em}}\lambda_c^2 + 4\lambda_c\right) \\ b_2 &= \left(10\sqrt{T_{em}}\lambda_c^3 + 6\lambda_c^2\right) \\ b_1 &= \left(5\sqrt{T_{em}}\lambda_c^4 + 4\lambda_c^3\right) \\ b_0 &= \left(\sqrt{T_{em}}\lambda_c^5 + \lambda_c^4 - \Gamma\right). \end{aligned} \tag{A4}$$

With the use of (A2), the last coefficient may be expressed as

$$b_0 = \left(1 - \frac{\sqrt{2}}{2}\right)\lambda_c^4.$$

Employing Montel's Theorem [27, p. 304], one root of (A4) must satisfy

$$|\delta| < 5\ \frac{\left(1 - \frac{\sqrt{2}}{2}\right)\lambda_c^4}{5\sqrt{T_{em}}\lambda_c^4 + 4\lambda_c^3}. \tag{A5}$$

A root locus analysis reveals that this root is the positive real root of (A3) and that $\delta < 0$. Simplifying (A5) via algebra then yields

$$\frac{\underline{z}}{\lambda_c} > 1 - \frac{\left(1 - \frac{\sqrt{2}}{2}\right)}{\sqrt{T_{em}}\lambda_c + \frac{4}{5}}.$$

Squaring both sides and noting that $\omega_c > \underline{\omega}_c$ provides the desired result

$$\frac{\omega_c}{\overline{\omega}_c} > \left(1 - \frac{\left(1 - \frac{\sqrt{2}}{2}\right)}{\lambda_c\sqrt{T_{em}} + \frac{4}{5}}\right)^2. \tag{A6}$$

The minimum value of the right hand side occurs for the case of no eddy currents ($T_{em} = 0$) indicating that $\omega_c/\overline{\omega}_c > 0.4$. However, we know in this case that $\omega_c/\overline{\omega}_c = 2^{-1/4} \approx 0.84$ so the upper bound $\overline{\omega}_c$ is tighter than (A6) indicates. Note that the bound (A6) becomes tighter as the effect of eddy currents (T_{em}) becomes greater.

A second lower bound may be developed by noting that $dN/dM > 1$. If the solution $\left(\overline{M}, \overline{N}\right)$ to (40), i.e., $N + M = \sqrt{2}\Gamma$, is projected along a line with $dN/dM = 1$ onto the curve $N^2 + M^2 = \Gamma^2$, the intersection point will yield a lower bound on ω_c in terms of $\overline{\omega}_c$. This, in turn, can be used to provide a guarantee on the tightness of the upper bound

$$\begin{aligned} \frac{\omega_c}{\overline{\omega}_c} &> \left(1 + \frac{\alpha^2}{2} - \sqrt{2}\left(\sqrt{1 + \sqrt{2}\alpha} - 1\right)\alpha\right)^{1/5} \\ \alpha &= \frac{1}{\lambda_c\sqrt{T_{em}}}. \end{aligned} \tag{A7}$$

Due to the method of derivation, this bound holds only for $0 < \alpha < 2+\sqrt{2}$. A numerical investigation reveals that lower bound (A7) is significantly tighter than (A6) for $\lambda_c\sqrt{T_{em}} > 0.5$, and that $\omega_c/\overline{\omega}_c > 0.75$ in such cases. From these investigations, we may conclude that the upper bound provided by (47) is sufficiently accurate for use in performance analysis.

REFERENCES

[1] R. Fittro and C. Knospe, "Rotor compliance minimization via mu-control of active magnetic bearings," *IEEE Trans. Control Syst. Technol.*, vol. 10, no. 2, pp. 238–249, Mar. 2002.

[2] H. Hayashiya, D. Iizuka, H. Ohsaki, and E. Masada, "A novel combined lift and propulsion system for a steel plate conveyance by electromagnets," *IEEE Trans. Magn.*, vol. 34, no. 4, pp. 2093–2095, Jul. 1998.

[3] D. L. Trumper, M. Weng, and R. Ritter, "Magnetic suspension and vibration control of beams for non-contact processing," presented at the IEEE Conf. Control Appl., Kona, HI, Aug. 1999.

[4] P. Subrahmanyan and D. Trumper, "Active vibration isolation design for a photolithographic stepper," in *Proc. 6th Int. Symp. Magn. Bearings*, 1998, pp. 10–21.

[5] H. Gutierrez and P. Ro, "Sliding-mode control of a nonlinear-input system: Application to a magnetically levitated fast-tool servo," *IEEE Trans. Ind. Electron.*, vol. 45, no. 6, pp. 921–927, Dec. 1998.

[6] R. L. Stoll, *The Analysis of Eddy Currents*. London, U.K.: Oxford Univ. Press, 1974.
[7] R. B. Zmood, D. K. Anand, and J. A. Kirk, "The influence of eddy currents on magnetic actuator performance," *Proc. IEEE*, vol. 75, no. 2, pp. 259–260, Feb. 1987.
[8] J. J. Feeley, "A simple dynamic model for eddy currents in a magnetic actuators," *IEEE Trans. Magn.*, vol. 32, no. 2, pp. 453–458, Mar. 1996.
[9] L. Kucera and M. Ahrens, "A model for axial magnetic bearings including eddy currents," presented at the 3rd Int. Symp. Magn. Suspension Technol., Tallahassee, FL, Dec. 1995.
[10] L. Zhu, C. Knospe, and E. Maslen, "An analytical model of a nonlaminated cylindrical magnetic actuator including eddy currents," *IEEE Trans. Magn.*, vol. 41, no. 4, pp. 1248–1258, Apr. 2005.
[11] L. Zhu, C. Knospe, and E. Maslen, "Frequency domain modeling of non-laminated C-shaped magnetic actuators," presented at the 9th Int. Symp. Magn. Bearings, Lexington, KY, Aug. 2004.
[12] L. Zhu and C. Knospe, "Modeling of non-laminated electromagnetic suspension systems," *IEEE/ASME Trans. Mechatron.*, vol. 15, no. 1, pp. 59–69, Feb. 2010.
[13] H. Bode, *Network Analysis and Feedback Amplifier Design*. New York: D. Van Nostrand Company, 1945.
[14] I. Horowiz, *Synthesis of Feedback Systems*. New York: Academic, 1963.
[15] J. Freudenberg and D. Looze, "Right half plane poles and zeros and design tradeoffs in feedback systems," *IEEE Trans. Autom. Control.*, vol. AC-30, no. 6, pp. 555–565, Jun. 1985.
[16] J. Freudenberg and D. Looze, "A sensitivity tradeoff for plants with time delay," *IEEE Trans. Autom. Control*, vol. AC-32, no. 2, pp. 99–104, Feb. 1987.
[17] R. H. Middleton, "Trade-offs in linear control systems design," *Automatica*, vol. 27, no. 2, pp. 281–292, Mar. 1991.
[18] M. Seron, J. Braslavsky, and C. Goodwin, *Fundamental Limitations in Filtering and Control*. New York: Springer, 1997.
[19] I. Podlubny, *Fractional Differential Equations*. San Diego, CA: Academic, 1999.
[20] K. Miller and B. Ross, *An Introduction to the Fractional Calculus and Fractional Differential Equations*. New York: Wiley, 1993.
[21] S. Samko, A. Kilbas, and O. Marichev, *Fractional Integrals and Derivatives: Theory and Applications*. New York: Taylor & Francis, 1993.
[22] D. Matignon, "Stability properties for generalized fractional differential systems," in *Proc. ESAIM*, 1998, vol. 5, pp. 145–158.
[23] C. Bonnet and J. R. Partington, "Coprime factorizations and stability of fractional differential systems," *Syst. Control Lett.*, vol. 41, no. 3, pp. 167–174, Oct. 2000.
[24] L. Zhu, "Non-laminated magnetic actuators: Modeling and performance limitations," Ph.D. dissertation, Dept. Mechan. Aerosp. Eng., Univ. Virginia, Blacksburg, 2005.
[25] V. Adamchik and D. Jeffrey, "Polynomial transformations of Tschirnhaus, Bring, and Jerrard," *ACM SIGSAM Bulletin*, vol. 37, no. 3, pp. 90–94, Sep. 2003.
[26] Wolfram Research, Champaign, IL, "MathWorld–A Wolfram Web Resource," 2010. [Online]. Available: http://library.wolfram.com/examples/quintic/main.html#diffeq
[27] Q. Rahman and G. Schmeisser, *Analytic Theory of Polynomials*. London, U.K.: Oxford Univ. Press, 2002.

Carl R. Knospe (SM'08) received the B.S. degree in aerospace engineering and the Ph.D. degree in mechanical and aerospace engineering from the University of Virginia, Charlottesville, in 1984 and 1989, respectively.

He is an Associate Professor with the Department of Mechanical and Aerospace Engineering, University of Virginia, Charlottesville, which he joined in 1989. His work has considered the active control of vibration, the design of high performance actuators, active magnetic suspension, the control of machining chatter, and the analysis of time delay systems. He is currently investigating microactuation. He is the author of over 40 journal publications and 60 conference publications.

Dr. Knospe has served as an Associate Editor for both IEEE TRANSACTIONS ON CONTROL SYSTEM TECHNOLOGY and *IEEE Control Systems Magazine*. He was a recipient of Best Paper Awards at both the 5th and 6th International Symposia on Magnetic Bearings (Kanazawa, Japan; Cambridge, MA).

Lei Zhu received the B.S. degree in electrical engineering from Hefei University of Technology, Hefei, China, in 1995, the M.S. degree in control engineering from the University of Science and Technology of China, Hefei, China, in 1998, and the Ph.D. degree in mechanical and aerospace engineering from the University of Virginia, Charlottesville, in 2005.

He is currently working on high speed rotating machinery supported by magnetic bearings at Calnetix Inc, Cerritos, CA. His research areas include electromechanical system design, analysis and control.